Atmos. Chem. Phys. Discuss., 13, 11971–11995, 2013
www.atmos-chem-phys-discuss.net/13/11971/2013/
doi:10.5194/acpd-13-11971-2013

Atmospheric Chemistry and Physics Discussions

The contribution of extratropical cyclones to observed cloud–aerosol relationships

B. S. Grandey[1,*], **P. Stier**[1], **R. G. Grainger**[1], **and T. M. Wagner**[1]

[1]Atmospheric, Oceanic and Planetary Physics, Department of Physics, University of Oxford, Oxford, UK
[*]now at: Singapore-MIT Alliance for Research and Technology, Singapore

Received: 24 January 2013 – Accepted: 12 April 2013 – Published: 7 May 2013

Correspondence to: B. S. Grandey (benjamin@smart.mit.edu)

Published by Copernicus Publications on behalf of the European Geosciences Union.

Abstract

Meteorological covariation may drive relationships between aerosol and cloud-related properties. It is important to account for the meteorological contribution to observed cloud–aerosol relationships in order to improve understanding of aerosol–cloud–climate interactions. A new method of investigating the contribution of meteorological covariation to observed cloud–aerosol relationships is introduced. Other studies have investigated the contribution of local meteorology to cloud–aerosol relationships. In this paper, a complimentary large-scale view is presented. Extratropical cyclones have been previously shown to affect satellite-retrieved aerosol optical depth (τ), due to enhanced emission of sea salt and sea surface brightness artefacts in regions of higher wind speed. Extratropical cyclones have also been shown to affect cloud-related properties such as cloud fraction (f_c) and cloud top temperature (T_{top}). Therefore, it seems plausible to hypothesise that extratropical cyclones may drive relationships between cloud-related properties and τ. In this paper, a description of extratropical cyclones, based on the relative vorticity of the storm and position in the storm domain, is used to analyse MODerate resolution Imaging Spectroradiometer (MODIS) retrieved τ, f_c and T_{top} data. This storm-centric description is capable of explaining f_c–τ relationships, although the relationships explained represent only a small component of the relationships observed in the MODIS data. This storm-centric approach produces no statistically robust explanation for T_{top}–τ relationships, suggesting that large-scale synoptic conditions in the mid-latitudes do not drive T_{top}–τ relationships. The primary causes for observed cloud–aerosol relationships are likely to be other factors such as retrieval errors, local meteorology or aerosol–cloud interactions.

1 Introduction

Much of the uncertainty in projections of future climate is associated with present-day aerosol radiative forcing (Andreae et al., 2005; Kiehl, 2007). Aerosol indirect effects

ACPD
13, 11971–11995, 2013

on clouds represent an important part of the climate system, but large uncertainties remain regarding the size of these effects (Lohmann and Feichter, 2005; Forster et al., 2007).

Strong relationships between aerosol and cloud-related properties have been observed. For example, positive relationships between total cloud fraction (f_c) and aerosol optical depth (τ) exist in data retrieved from the MODerate resolution Imaging Spectroradiometer (MODIS) instrument (Koren et al., 2005; Kaufman et al., 2005; Grandey et al., 2013). Similarly, positive relationships between cloud top height and τ have also been observed (Koren et al., 2005).

Many causal mechanisms potentially may be able to explain these observed relationships (Stevens and Feingold, 2009; Grandey et al., 2013). For example, meteorological conditions may drive relationships between aerosol and cloud-related properties. Ten-metre wind speed can explain a large part of observed f_c–τ correlations (Engström and Ekman, 2010). Additionally, covariation with humidity can lead to positive f_c–τ relationships (Quaas et al., 2010; Chand et al., 2012; Grandey et al., 2013). Most previous studies which consider potential meteorological contributions to observed aerosol–cloud relationships, including those mentioned above, have looked at simple local meteorological variables such as relative humidity and wind speed. Large-scale synoptic conditions are an important factor affecting local meteorology. Therefore, large-scale synoptic systems may lead to correlations between aerosols and clouds, potentially organising spatiotemporal patterns in cloud-aerosol relationships.

Many studies have shown that extratropical cyclones and fronts are major drivers of large-scale cloud-related properties (Lau and Crane, 1995, 1997; Norris and Iacobellis, 2005; Wang and Rogers, 2001; Chang and Song, 2006; Field and Wood, 2007; Field et al., 2008). The high wind speeds associated with extratropical cyclones can increase sea salt emission and introduce surface brightness artefacts to satellite retrievals, increasing the aerosol optical depth (Grandey et al., 2011). Since extratropical cyclones have been shown to affect cloud-related properties and τ, it seems credible to hypothesise that extratropical cyclones may drive relationships between cloud-related

ACPD
13, 11971–11995, 2013

properties and τ. Here, the storm-centric compositing methodology is applied to the investigation of observed relationships between aerosols and clouds. The relative vorticity of each storm and position relative to the storm centre are considered in order to provide a simplified description of the large-scale forcing of aerosols and clouds by extratropical cyclones. The following question is considered in this paper: can relationships between aerosol and cloud-related properties be explained by considering simply the relative vorticity of extratropical cyclones and position relative to the storm centre?

The data and methodology used are explained in Sect. 2. Results are presented and discussed in Sect. 3. Conclusions are summarised in Sect. 4.

2 Method

This paper uses daytime data from the MODIS Science Team Collection 5 Atmosphere Level 2 Joint Product for the Aqua satellite (MTDATML2) (Platnick et al., 2003; Remer et al., 2005). In addition to the 10 km × 10 km aerosol optical depth (τ) data used in Grandey et al. (2011), this paper also uses 5 km × 5 km cloud fraction (f_c) and cloud top temperature (T_{top}) data. Liquid cloud top properties, such as liquid cloud droplet number concentration, are not investigated here. Strict ocean-retrieval-only masking is applied to the τ data only. Retrievals of f_c and T_{top} are likely to be far less sensitive to surface albedo changes between land and ocean, although the T_{top} of thin or broken clouds may sometimes be contaminated by surface emissivities which differ between land and ocean. As in Grandey et al. (2011), 1.5° × 1.5° ERA-Interim 850 hPa relative vorticity (ω), zonal and meridional components of the 10-metre wind and mean sea level pressure are also used. All data cover 2003–2007.

The storm-centric gridding methodology is almost identical to that explained in Grandey et al. (2011). Extratropical cyclones are tracked using TRACK (Hodges, 1995, 1999). Here, the level 2 satellite data and the ERA-Interim data are gridded to a resolution of 200 km × 200 km. This seems to be a reasonable choice of co-location scale for much of the aerosol–cloud interaction analysis. At this scale, the assumption of clear-

ACPD
13, 11971–11995, 2013

sky τ being representative for the grid box should hold, such that the τ data generally can be assumed to be co-located with the f_c and T_{top} data, although individual pollution plumes may occur on smaller scales (Anderson et al., 2003; Weigum et al., 2012). It is worth noting that satellite-retrieved τ data are for clear-sky conditions, because aerosol retrievals require pixels that have been flagged as cloud-free, although some cloud contamination of τ may remain.

In order to illustrate how τ, f_c and T_{top} change between weaker and stronger storms, median composites for a weaker relative vorticity range of $3 < \omega < 5\times10^{-5}\,s^{-1}$ are shown alongside those for the stronger vorticity range of $\omega > 7\times10^{-5}\,s^{-1}$ used in Grandey et al. (2011). These median composites are constructed by calculating the median value within each storm-centric grid box. The weaker vorticity range was chosen to sample a similar number of storms to the stronger vorticity range. To provide an indication of the data spread within each of these vorticity ranges, lower and upper quartile composites are produced to complement the median composites. For example, Fig. 1 shows the τ composites for the North Atlantic ocean (NA). Figure 2 shows the corresponding f_c composites. The median storm-centre mean sea level pressures are 1008 hPa for the weaker range and 988 hPa for the stronger range.

Alongside the storm-centric regridding, the data are also regridded with respect to storm tracks which have have been translated temporally by one year, creating all-conditions data (Grandey et al., 2011). These all-conditions data should be representative of average conditions. They are blind as to whether or not a storm is present in the domain, but they retain the same seasonal and locational sampling as the storm-centric data.

Regression slopes and correlations of the cloud-related properties versus τ are calculated for the all-conditions data and for the storm-centric data. This is done for each 200 km × 200 km grid box in the domain. The full range of vorticities, $\omega > 1\times10^{-5}\,s^{-1}$, are used for the regression and correlation calculations. Linear fits are used for T_{top} versus τ and for f_c versus $\ln\tau$ based on semi-empirical considerations, including analysis of the coefficient of determination (Chapter 3 of Grandey, 2011). For example, the

ACPD
13, 11971–11995, 2013

regression slopes and correlations of NA f_c versus τ are shown in the first and third columns of Fig. 3.

In order to investigate the extent to which storm strength may be able to explain the observed relationships, the τ and cloud property data are shuffled for each grid box within narrow vorticity ranges of $1\times10^{-5}\,s^{-1}$ before recalculating the regression slopes and correlations. By randomising the pairing of the cloud and τ data before calculating the relationships, the contributions due to retrieval errors and aerosol–cloud interactions are largely removed. However, they may not be completely removed because some correctly matched cloud property and τ pairs may remain after shuffling, most likely for stronger storms with $\omega > 10\times10^{-5}\,s^{-1}$ where there are fewer storms in a given $1\times10^{-5}\,s^{-1}$ interval (Table 1). Because this shuffling occurs within narrow ω ranges, the shuffled cloud and τ data remain functions of ω. So the calculated relationships between shuffled τ and the cloud properties represent the synoptic component which can be explained by ω and position in the storm-centric domain. Of course, no strong relationships should be found for the shuffled all-conditions data which are also included as a control. For example, the second and fourth columns of Fig. 3 show the regression slopes and correlations of NA f_c versus τ, where the data were first shuffled within each narrow vorticity range.

Most of the results for North Atlantic ocean (NA; 50–10° W, 30–55° N) storms are shown and discussed in this paper. Some of the corresponding results for the South Atlantic ocean (SA; 50° W–10° E, 55° S–30° S) are shown in the Supplement. The SA results, which are generally similar to those for the NA, are also discussed briefly in the main body of this paper.

ACPD
13, 11971–11995, 2013

3 Results and discussion

3.1 Aerosol optical depth (τ)

Figure 1a–c shows the lower quartile, median and upper quartile storm-centric composites of Aqua-MODIS Collection 5 Aerosol Optical Depth (τ) for North Atlantic ocean (NA) storms with relative vorticity (ω) in the range $3 < \omega < 5\times10^{-5}\,s^{-1}$. The lower quartile composite has low τ across most of the domain, with a slight enhancement in the region of high wind speeds to the south-east of the storm centre. There is also a slight enhancement in the south-east corner of the domain, far away from the storm-centre, most likely due to background conditions in the NA. In the median composite, a slight enhancement is also visible just to the south-east of the storm centre, but is weak compared to the background. A decrease in the south-western and northern parts of the domain is visible in the median composite, likely due in part to the low wind speeds here, although frontal clearance, subsidence behind the front and the advection of polar air may also play a role. This decrease is more striking in the upper quartile composite, showing that high τ values are uncommon to the north-west of the storm centre and in the south-western part of the domain for this vorticity range.

Figure 1d–f shows corresponding composites for a stronger vorticity range of $\omega > 7\times10^{-5}\,s^{-1}$. A strong enhancement of τ in the regions of high wind speed to the south and east of the storm centre is visible in both the lower quartile and the upper quartile composites in addition to the median composite. This storm-centric enhancement is due to a combination of wind speed dependent surface brightness artefacts and increased emission of sea salt (Grandey et al., 2011). The enhancement is much stronger for the stronger vorticity range than it is for the weaker vorticity range.

For both vorticity ranges, there is an average τ increase of approximately 0.05 between the lower quartile and median composites, and an increase of approximately 0.07 between the median and the upper quartile composites. This is quite a large spread compared to the average enhancement of less than 0.01 due to the change in vorticity. However, near the centre of the storm domain, the signal due to the vortic-

ACPD
13, 11971–11995, 2013

ity change is approximately 0.05, comparable to the average differences between the medians and the quartiles.

The corresponding South Atlantic ocean (SA) composites can be seen in Fig. S1 of the Supplement. The latitudes have been inverted, with the poleward (southward) direction pointing to the top of the page. They are similar to those for the NA, but with a lower background τ level (Grandey et al., 2011).

3.2 Cloud fraction (f_c)

The lower quartile, median and upper quartile storm-centric composites of Aqua-MODIS Collection 5 cloud fraction (f_c) for storms with vorticity in the range $3 < \omega < 5\times10^{-5}\,s^{-1}$ are shown in Fig. 2a–c. Blue indicates low f_c while red indicates high f_c. It can be seen there are often very high f_c values in the polewards part and the centre of the storm domain. Even in the lower quartile, f_c values larger than 0.8 are observed towards the centre of the storm domain. This feature corresponds to the cloud shield with cold T_{top} commented on in Sect. 3.3 below. In the upper quartile, the entire domain contains large f_c values, with the upper quartile composite domain mean being 0.965.

It is worth noting that these large fractional cloud covers may affect τ data in two ways. First, no aerosol retrievals will occur for grid boxes with complete cloud cover, biasing the τ data towards situations with lower f_c values. This is because aerosol retrievals require cloud-free pixels. Second, cloud contamination of τ may be correlated with f_c. However, the τ composites do not show a general meridional gradient in τ, only an enhancement near the storm centre, whereas the f_c composites show a strong meridional gradient. This suggests that potential cloud contamination alone cannot explain the observed τ composites shown in Fig. 1. However, it is possible that cloud contamination may still contribute towards observed relationships between aerosol and cloud-related properties, as discussed in Grandey et al. (2013).

Figure 2d–f shows the lower quartile, median and upper quartile storm-centric f_c composites for the stronger vorticity range of $\omega > 7\times10^{-5}\,s^{-1}$. It can be seen from the

ACPD
13, 11971–11995, 2013

mean sea level pressure contours, shown in white, that deeper pressure minima occur for these stronger storms. These composites have similar spatial patterns to those for the weaker vorticity range, but with higher values of f_c. The domain mean f_c differences between the two vorticity ranges are approximately 0.1, 0.07 and 0.02 for the lower quartile, median and upper quartile composites respectively. This shows that storm strength can have a large effect on f_c. However, the domain mean differences between the lower quartile and the median, approximately 0.2–0.3, and between the median and upper quartile, approximately 0.1, show that there is also a large variation within each of these vorticity ranges.

It has been demonstrated that both τ and f_c generally increase with storm strength, suggesting that the large-scale synoptic conditions of extratropical cyclones may lead to relationships between these two variables. Quantitative relationships between τ and f_c are now investigated.

Figure 3a shows the all-conditions regression slopes of f_c versus $\ln\tau$. Positive slopes, shown in red, are observed everywhere in the all-conditions domain. Every grid box has a statistically significant f_c versus $\ln\tau$ regression slope, as shown by the ubiquitous stippling.

The corresponding storm-centric regression slopes, shown in Fig. 3e, are similarly significant. The storm-centric regression slopes are very similar to those for all-conditions. There is a slight weakening in the centre of the storm domain, possibly due to there being little variation in the high f_c values found here. The error-weighted mean (EWM) is very slightly smaller, being 0.163 compared to 0.165. The errors on these EWMs are more than two orders of magnitude smaller than the EWMs themselves.

As outlined in Sect. 2, the f_c and τ data for each grid box are next shuffled within each vorticity range of $1\times10^{-5}\,s^{-1}$. The regression slopes are then recalculated across the full vorticity range. The NA all-conditions results are shown in Fig. 3b. A mixture of positive and negative slopes are observed. The random shuffling largely removes correlations between f_c and τ induced by indirect effects and correlated retrieval errors. The simplified large-scale synoptic contribution described by ω and position in the

ACPD
13, 11971–11995, 2013

storm domain is retained. Since ω and position are meaningless references for the all-conditions data, it should be expected that the shuffled all-conditions slopes should be approximately zero. The magnitude of the EWM is larger than the one-sigma error. However, it is two orders of magnitude smaller than the all-conditions EWM for the non-shuffled data and is also opposite in sign, −0.001 compared to 0.165.

Figure 3f shows the regression slopes for the shuffled NA storm-centric data. Many individual slopes just to the south and west of the domain centre are positive and significant, suggesting that the simplified description of the large-scale synoptics investigated here may indeed explain a contribution to observed relationships between f_c and τ. This part of the domain, to the south of the storm centre, is also where the winds are strongest. The significant EWM of 0.004, which is also larger than the all-conditions EWM of −0.001, also supports this suggestion. However, this EWM is still almost two orders of magnitude smaller than the non-shuffled EWM of 0.163. Although the simplified large-scale synoptics, described by storm vorticity and position in the storm domain, may explain a contribution to relationships between f_c and τ, this contribution is very small compared to the total observed f_c–$\ln\tau$ relationships.

Similar conclusions can be made for the f_c–$\ln\tau$ correlation coefficients. The all-conditions and storm-centric correlation coefficients, shown in Fig. 3c and g, are very similar to each other and are consistently positive. The correlations for the shuffled NA all-conditions f_c and $\ln\tau$ data, shown in Fig. 3d, are more than two orders of magnitude smaller. The mean of −0.002 has an opposite sign to that for the non-shuffled all-conditions data and is close to zero, consistent with the regression slopes. The correlations for the shuffled storm-centric data, shown in Fig. 3h, are mostly positive, particularly near the storm centre. The mean of 0.011 is stronger than that for the shuffled all-conditions data, but it is still much smaller than the correlations for the non-shuffled data. Again, this suggests that the simplified description of the synoptics categorised here may be capable of explaining a contribution to relationships between f_c and $\ln\tau$, but this contribution is much smaller than the total observed relationships.

ACPD
13, 11971–11995, 2013

The SA f_c composites (not shown) are very similar to those for the NA. The f_c–$\ln\tau$ regression slope and correlation results for the SA are shown in Fig. S2 of the Supplement. The latitudes have been inverted. One difference compared to the NA is that there is a stronger meridional gradient in the regression slopes. Apart from this difference, the results are very similar to those for the NA. They provide further support for the conclusion that the simplified description of the large-scale synoptics can explain relationships between τ and f_c.

3.3 Cloud top temperature (T_{top})

Figure 4a–c show the lower quartile, median and upper quartile storm-centric composites of Aqua-MODIS Collection 5 cloud top temperature (T_{top}) for NA storms with relative vorticity in the range $3 < \omega < 5\times10^{-5}\,s^{-1}$. The lower quartile tends towards sampling scenes where cold high cloud dominates, whereas the upper quartile tends towards scenes where warm low cloud can be seen. A shield of colder higher cloud can be discerned to the east of the storm centre in all three of the composites. Relatively cold cloud can also be seen in the advected cold polar air in the north-west of the storm-centric domain. In the lower quartile, a band of warmer cloud can be seen to the west of the storm centre, indicating a general absence of high clouds here. A general meridional gradient in T_{top} exists, with warmer clouds generally observed at the equatorward edge of the domain.

The composites for the stronger vorticity range of $\omega > 7\times10^{-5}\,s^{-1}$ are shown in Fig. 4d–f. These composites have similar general features to those for the weaker vorticity range. The shield of cold high cloud is larger and colder for the stronger vorticity range than it is for the weaker vorticity range. This is to be expected, since this shield of high cloud is synoptically driven.

Field and Wood (2007) presented a NA T_{top} mean composite plot. They used a different storm identification and compositing methodology to that used here, identifying extratropical cyclones based on surface pressure gradients and minima. Their mean

ACPD
13, 11971–11995, 2013

composite of T_{top} has similar features to the median composites produced here and shown in Fig. 4. The T_{top} values of the Field and Wood (2007) composite are somewhere between those for the two vorticity ranges used here. Similarly, their mean storm-centre mean sea level pressure of approximately 1000 hPa is between the median storm-centre values of 1008 hPa and 988 hPa for the NA composites produced here.

For both vorticity ranges, the domain average increase in T_{top} between the lower quartile and the median is approximately 17 K. The increase between the median and the upper quartile is approximately 10 K. The domain average decrease between the weaker composites and the stronger composites is approximately 5 K, considerably smaller than the spread between the quartiles. However, the strengthening of the high cloud shield can result in some grid boxes seeing decreases of up to 20 K.

Figure 5a shows the regression slopes of T_{top} versus τ for each grid box of the NA all-conditions gridded data. It can be seen that negative regression slopes, indicated by blue, are found almost everywhere in the domain. Taken individually, almost all of these regression slopes are statistically insignificant at two-sigma confidence, indicated by the lack of stippling. However, the EWM for the whole domain is an order of magnitude larger than the associated one-sigma error.

The corresponding storm-centric regression slopes are shown in Fig. 5e. As mentioned in Sect. 2, the full vorticity range of all tracked storms is used. It can be seen that the storm-centric regression slopes are very similar to those for all-conditions. The storm-centric EWM of −15.2 K is slightly steeper than the all-conditions EWM of −14.9 K. However, the one-sigma error of 0.9 K suggests that this smaller difference may be insignificant. This shows that analysing relationships between NA T_{top} and τ in a storm-centric context appears to make little discernible difference to the results.

As outlined in Sect. 2, the T_{top} and τ data are next shuffled for each grid box within narrow vorticity ranges of $1\times10^{-5}\,s^{-1}$. The regression slopes are then recalculated. It would be expected that these regression slopes for the shuffled all-conditions data should be statistically indistinguishable from zero. This is indeed the case, as Fig. 5b shows. The all-conditions slope EWM of 0.1 K is an order of magnitude smaller than

ACPD
13, 11971–11995, 2013

that for the non-shuffled all-conditions data and it is much smaller than the associated one-sigma error of 0.9 K, rendering it insignificantly different from zero.

The slopes for the shuffled storm-centric data, shown in Fig. 5f, are also very small. The EWM of −0.2 K is slightly steeper than for the shuffled all-conditions data, but it is still much smaller than both the one-sigma error and the non-shuffled EWM. These results show that there is no evidence to suggest that large-scale ω and position relative to the storm centre, representing a simplified description of synoptic forcing by extratropical cyclones, can explain relationships between τ and T_{top}.

The all-conditions and storm-centric correlation coefficients, shown in Fig. 5c and g, are also very similar to one another. The observed correlations are negative, approximately −0.2 on average. The correlations for the shuffled all-conditions and storm-centric data are shown in Fig. 5d and h. They are two orders of magnitude smaller than for the non-shuffled data. These observations for the correlation coefficients are consistent with those made for the regression slopes.

The SA T_{top} composites (not shown) are very similar to those for the NA. Regression slopes and correlations for the SA are shown in Fig. S3 of the Supplement. The EWM regression slopes for the non-shuffled data are stronger for the SA than for the NA, and there is a stronger meridional gradient, with the slopes becoming steeper nearer the equator. As was the case for the NA results, the difference between the all-conditions and the storm-centric EWM regression slopes is statistically insignificant, being smaller than the one-sigma error. Although the storm-centric shuffled regression slope EWM of −0.7 K is steeper than for the NA, it is still statistically insignificant. Similar remarks can be made for the SA correlations as were made for the NA correlations. Again, there is no evidence to suggest that the simplified description of large-scale synoptic forcing, described by ω and position in storm domain, can explain relationships between τ and T_{top}.

ACPD
13, 11971–11995, 2013

4 Conclusions

In Grandey et al. (2011), it was shown that extratropical cyclones affect Aqua-MODIS retrieved aerosol optical depth (τ) over ocean. This paper has further demonstrated that on average for a given position in the storm-centric domain, stronger storms generally lead to higher τ than weaker storms, particularly near the storm centre. However, this enhancement is generally smaller than the variability in τ for a given storm strength and position in the storm-centric domain, probably due to variations in local wind speeds.

Storm-centric composites of cloud-related properties have been investigated in this paper, building on the previous work of Lau and Crane (1995, 1997), Norris and Iacobellis (2005), Wang and Rogers (2001), Chang and Song (2006), Field and Wood (2007) and Field et al. (2008). Median composites of cloud fraction (f_c) show a general increase in f_c with storm strength. However, as for the τ fields, the variability between the quartiles for a given storm strength is generally larger than the difference between different storm strengths.

Cloud top temperature (T_{top}) composites reveal a cold high cloud shield to the north and east of the storm centre. The extent and height of this shield increases with storm strength. The domain average T_{top} is colder for stronger storms compared to weaker storms. However, once again the variability between the quartiles for a given storm strength is generally larger than the difference due to vorticity changes, except for some grid boxes near the centre of the storm domain.

Because storm strength has been shown to affect τ, f_c and T_{top}, it seemed plausible to hypothesize that extratropical cyclones may cause relationships between these three properties. Storm-centric regression slopes and correlation coefficients of f_c versus $\ln\tau$ and T_{top} versus τ have been calculated. Positive f_c–$\ln\tau$ and negative T_{top}–τ relationships are observed.

The τ, f_c and T_{top} data have subsequently been shuffled within narrow ranges of storm vorticity, prior to recalculating the regressions slopes and correlations. This has been done in an attempt to remove correlations due to retrieval errors and genuine

ACPD
13, 11971–11995, 2013

aerosol–cloud interactions. By choosing narrow ranges of storm vorticity and retaining position in the storm domain, a simplified description of the large-scale synoptics of extratropical cyclones has been investigated. This has been done in order to answer the question asked at the beginning of the paper: can relationships between aerosol and cloud-related properties be explained by considering simply the relative vorticity of extratropical cyclones and position relative to the storm centre?

The f_c versus $\ln\tau$ regression slopes for the shuffled data are often found to be significant. This suggests that the storm-centric description of the large-scale synoptics can explain relationships between f_c and τ. However, these relationships are far smaller than observed relationships between f_c and τ, which may be better explained by cloud contamination, relative humidity (Quaas et al., 2010; Chand et al., 2012; Grandey et al., 2013) and descriptions of meteorology based on local field variables such as winds (Engström and Ekman, 2010). Many of the significant slopes are found just to the south of the storm centre, where the winds are generally strongest. This suggests that the synoptically induced winds, which were largely found to explain the observed storm-centric τ composites (Grandey et al., 2011), may be the mechanism by which the storm-centric large-scale synoptics can explain relationships between f_c and τ.

The T_{top} versus τ regression slopes for the shuffled data are insignificant, even when averaged across the storm-centric domain. This demonstrates that the storm-centric description of the synoptics, described by storm vorticity and position relative to the storm centre, is incapable of explaining relationships between T_{top} and τ for the data used here. This suggests that large-scale synoptic conditions in the mid-latitudes are not a major driver of T_{top}–τ relationships. Further research is needed to identify the contributions of satellite retrieval errors, local meteorology and aerosol–cloud interactions to observed T_{top}–τ relationships.

As an alternative to using local meteorological field variables to account for relationships between aerosol and cloud-related properties, this paper has introduced the possibility of considering large-scale synoptic systems instead. The approach used, whereby data are categorised according to position in the storm-centric domain and

ACPD
13, 11971–11995, 2013

storm vorticity, has proved to be partially successful. A combination of the storm-centric and local meteorological variable approaches might be more fruitful than either approach taken in isolation. Cloud and aerosol data could be categorised by position in the storm-centric domain and a local meteorological variable, providing a basis for future work. A complementary approach may be to consider cloud regimes, as has been done by Gryspeerdt and Stier (2012) for the investigation of relationships between liquid cloud droplet number concentration and τ.

Supplementary material related to this article is available online at: http://www.atmos-chem-phys-discuss.net/13/11971/2013/acpd-13-11971-2013-supplement.pdf.

Acknowledgements. MODIS data were obtained from the Level 1 and Atmosphere Archive and Distribution System (LAADS). ERA-Interim data were obtained from the European Centre for Medium-Range Weather Forecasts (ECMWF). The TRACK code and configuration were provided by Kevin Hodges. This work was supported by a UK Natural Environment Research Council (NERC) DPhil studentship and also the NERC AEROS project (NE/G006148/1). The research leading to these results has also received funding from the European Research Council under the European Union's Seventh Framework Programme (FP7/2007–2013)/ERC grant agreement no. FP7-280025. RGG acknowledges funding from the NERC National Centre for Earth Observation. Thanks are due to Joanna Eberhardt who commented on an earlier draft of this paper.

References

Anderson, T. L., Charlson, R. J., Winker, D. M., Ogren, J. A., and Holmén, K.: Mesoscale variations of tropospheric aerosols, J. Atmos. Sci., 60, 119–136, 2003. 11975

Andreae, M. O., Jones, C. D., and Cox, P. M.: Strong present-day aerosol cooling implies a hot future, Nature, 435, 1187–1190, doi:10.1038/nature03671, 2005. 11972

ACPD
13, 11971–11995, 2013

Chand, D., Wood, R., Ghan, S. J., Wang, M., Ovchinnikov, M., Rasch, P. J., Miller, S., Schichtel, B., and Moore, T.: Aerosol optical depth increase in partly cloudy conditions, J. Geophys. Res., 117, D17207, doi:10.1029/2012JD017894, 2012. 11973, 11985

Chang, E. K. M. and Song, S.: The seasonal cycles in the distribution and precipitation around cyclones in the Western North Pacific and Atlantic, J. Atmos. Sci., 63, 815–839, 2006. 11973, 11984

Engström, A. and Ekman, A. M. L.: Impact of meteorological factors on the correlation between aerosol optical depth and cloud fraction, Geophys. Res. Lett., 37, L18814, doi:10.1029/2010GL044361, 2010. 11973, 11985

Field, P. R. and Wood, R.: Precipitation and cloud structure in midlatitude cyclones, J. Climate, 20, 233–254, doi:10.1175/JCLI3998.1, 2007. 11973, 11981, 11982, 11984

Field, P. R., Gettelman, A., Neale, R. B., Wood, R., Rasch, P. J., and Morrison, H.: Midlatitude cyclone compositing to constrain climate model behaviour using satellite observations, J. Climate, 21, 5887–5903, doi:10.1175/2008JCLI2235.1, 2008. 11973, 11984

Forster, P., Ramaswamy, V., Artaxo, P., Berntsen, T., Betts, R., Fahey, D. W., Haywood, J., Lean, J., Lowe, D. C., Myhre, G., Nganga, J., Prinn, R., Raga, G., Schultz, M., and Van Dorland, R.: Changes in atmospheric constituents and in radiative forcing, in: Climate Change 2007: The Physical Science Basis. Contribution of Working Group 1 to the Fourth Assessment Report of the Intergovernmental Panel on Climate Change, Cambridge University Press, 129–234, 2007. 11973

Grandey, B. S.: Investigating aerosol–cloud interactions, Ph.D. thesis, University of Oxford, UK, available at: http://ora.ox.ac.uk/objects/uuid:8b48c02b-3d43-4b04-ae55-d9885960103d, 2011. 11975

Grandey, B. S., Stier, P., Wagner, T. M., Grainger, R. G., and Hodges, K. I.: The effect of extratropical cyclones on satellite-retrieved aerosol properties over ocean, Geophys. Res. Lett., 38, L13805, doi:10.1029/2011GL047703, 2011. 11973, 11974, 11975, 11977, 11978, 11984, 11985

Grandey, B. S., Stier, P., and Wagner, T. M.: Investigating relationships between aerosol optical depth and cloud fraction using satellite, aerosol reanalysis and general circulation model data, Atmos. Chem. Phys., 13, 3177–3184, doi:10.5194/acp-13-3177-2013, 2013. 11973, 11978, 11985

Gryspeerdt, E. and Stier, P.: Regime-based analysis of aerosol-cloud interactions, Geophys. Res. Lett., 39, L21802, doi:10.1029/2012GL053221, 2012. 11986

ACPD
13, 11971–11995, 2013

Hodges, K. I.: Feature tracking on the unit sphere, Mon. Weather Rev., 123, 3458–3465, 1995. 11974
Hodges, K. I.: Adaptive constraints for feature tracking, Mon. Wea. Rev., 127, 1362–1373, 1999. 11974
Kaufman, Y. J., Koren, I., Remer, L. A., Rosenfeld, D., and Rudich, Y.: The effect of smoke, dust, and pollution aerosol on shallow cloud development over the Atlantic Ocean, P. Natl. Acad. Sci. USA, 102, 11207–11212, doi:10.1073/pnas.0505191102, 2005. 11973
Kiehl, J. T.: Twentieth century climate model response and climate sensitivity, Geophys. Res. Lett., 34, L22710, doi:10.1029/2007GL031383, 2007. 11972
Koren, I., Kaufman, Y. J., Rosenfeld, D., Remer, L. A., and Rudich, Y.: Aerosol invigoration and restructuring of the Atlantic convective clouds, Geophys. Res. Lett., 32, L14828, doi:10.1029/2005GL023187, 2005. 11973
Lau, N.-C. and Crane, M. W.: A satellite view of the synoptic-scale organization of cloud properties in midlatitude and tropical circulation systems, Mon. Wea. Rev., 123, 1984–2006, 1995. 11973, 11984
Lau, N.-C. and Crane, M. W.: Comparing satellite and surface observations of cloud patterns in synoptic-scale circulation systems, Mon. Wea. Rev., 125, 3172–3189, 1997. 11973, 11984
Lohmann, U. and Feichter, J.: Global indirect aerosol effects: a review, Atmos. Chem. Phys., 5, 715–737, doi:10.5194/acp-5-715-2005, 2005. 11973
Norris, J. R. and Iacobellis, S. F.: North Pacific cloud feedbacks inferred from synoptic-scale dynamic and thermodynamic relationships, J. Climate, 18, 4862–4878, 2005. 11973, 11984
Platnick, S., King, M. D., Ackerman, S. A., Menzel, W. P., Baum, B. A., Riedi, J. C., and Frey, R. A.: The MODIS cloud products: algorithms and examples from terra, IEEE T. Geosci. Remote, 41, 459–473, doi:10.1109/TGRS.2002.808301, 2003. 11974
Quaas, J., Stevens, B., Stier, P., and Lohmann, U.: Interpreting the cloud cover – aerosol optical depth relationship found in satellite data using a general circulation model, Atmos. Chem. Phys., 10, 6129–6135, doi:10.5194/acp-10-6129-2010, 2010. 11973, 11985
Remer, L. A., Kaufman, Y. J., Tanré, D., Mattoo, S., Chu, D. A., Martins, J. V., Li, R.-R., Ichoku, C., Levy, R. C., Kleidman, R. G., Eck, T. F., Vermote, E., and Holben, B. N.: The MODIS Aerosol Algorithm, Products, and Validation, J. Atmos. Sci., 62, 947–973, doi:10.1175/JAS3385.1, 2005. 11974
Stevens, B. and Feingold, G.: Untangling aerosol effects on clouds and precipitation in a buffered system, Nature, 461, 607–613, doi:10.1038/nature08281, 2009. 11973

ACPD
13, 11971–11995, 2013

Wang, C.-C. and Rogers, J. C.: A composite study of explosive cyclogenesis in different sectors of the North Atlantic, Part I: Cyclone structure and evolution, Mon. Wea. Rev., 129, 1481–1499, 2001. 11973, 11984

Weigum, N. M., Stier, P., Schwarz, J. P., Fahey, D. W., and Spackman, J. R.: Scales of variability of black carbon plumes over the Pacific Ocean, Geophys. Res. Lett., 39, L15804, doi:10.1029/2012GL052127, 2012. 11975

ACPD

13, 11971–11995, 2013

Table 1. Minimum, mean and maximum number of cloud–τ data pairs per storm-centric 200 km × 200 km grid box for different 850 hPa relative vorticity (ω) ranges over the North Atlantic ocean.

ω range ($\times 10^{-5}$ s^{-1})	Number of cloud–τ data pairs per grid box		
	Minimum	Mean	Maximum
3–5	277	530.0	669
> 7	188	461.6	622
1–2	120	265.7	346
2–3	112	254.8	338
3–4	130	286.2	378
4–5	147	243.9	309
5–6	133	240.5	303
6–7	81	165.7	223
7–8	42	114.1	151
8–9	19	58.9	88
9–10	8	32.7	54
10–11	3	15.7	35
11–12	2	9.2	23
12–13	0	2.4	9
13–14	0	2.3	10
14–15	0	1.3	4

ACPD
13, 11971–11995, 2013

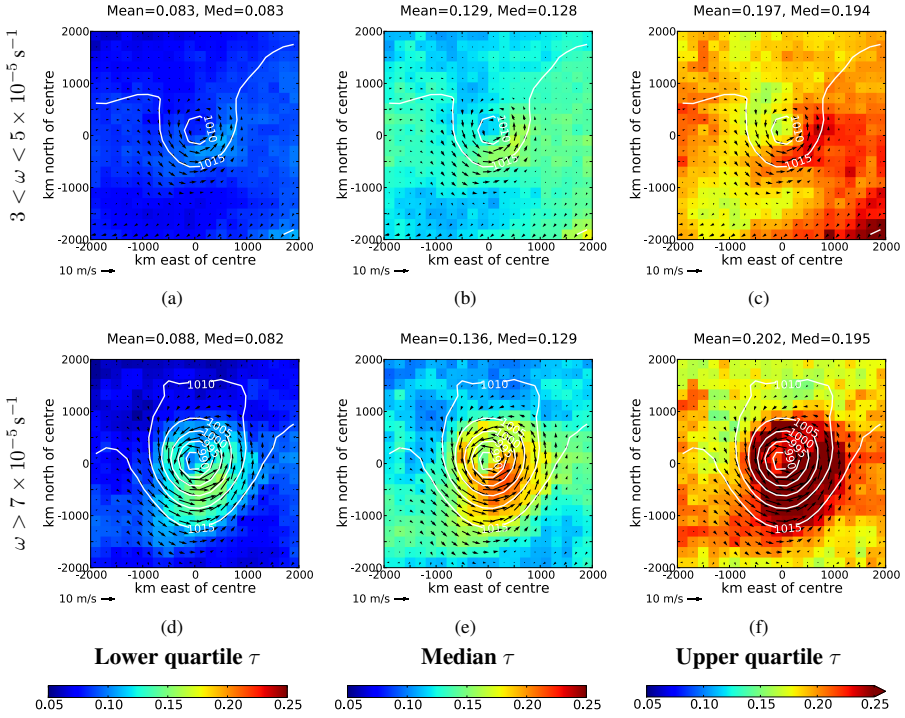

Fig. 1. Storm-centric **(a, d)** lower quartile, **(b, e)** median and **(c, f)** upper quartile composites of Aqua-MODIS aerosol optical depth (τ) for two 850 hPa relative vorticity (ω) ranges over the North Atlantic ocean. Median composites of ERA-Interim mean sea level pressure (p_0; white contours) and wind vectors (black arrows) are over-plotted. The wind vector scale is provided at the bottom left-hand edge of each composite. Positive meridional displacements are poleward of the storm centre. The data cover 2003–2007.

ACPD
13, 11971–11995, 2013

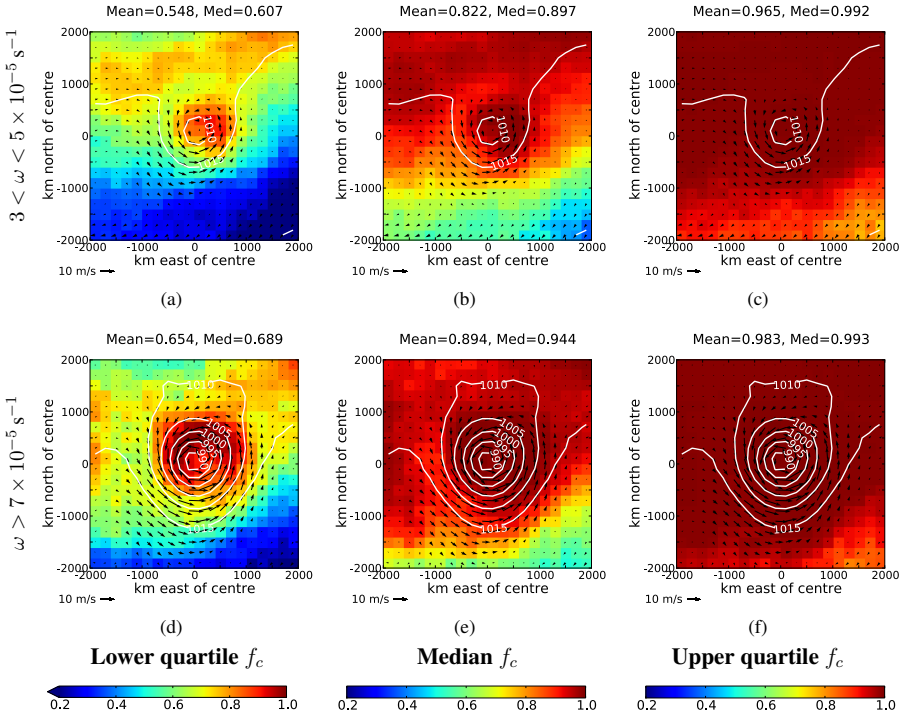

Fig. 2. Similar to Fig. 1, but for Aqua-MODIS cloud fraction (f_c) over the North Atlantic ocean.

ACPD
13, 11971–11995, 2013

Contribution of cyclones to cloud–aerosol relationships

B. S. Grandey et al.

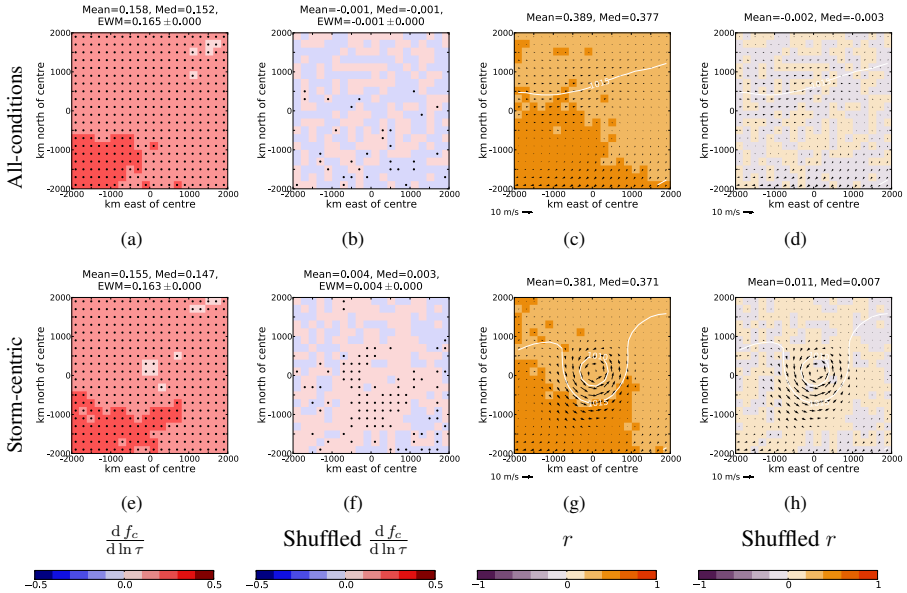

Fig. 3. (a) All-conditions results of an ordinary least squares regression fit of Aqua-MODIS cloud fraction (f_c) versus ln aerosol optical depth ($\ln\tau$) over the North Atlantic ocean. **(b)** Similar to **(a)**, but for f_c and $\ln\tau$ data which have been shuffled within each narrow relative vorticity range. Non-stippled slopes are statistically insignificant at the two-sigma confidence level. **(c)** Linear Pearson correlation coefficients (r) corresponding to the slopes shown in **(a)**. Median composites of ERA-Interim mean sea level pressure (p_0; white contours) and wind vectors (black arrows) are over-plotted. **(d)** Correlation coefficients corresponding to the slopes of the shuffled data shown in **(b)**. **(e–g)** Similar to **(a–d)**, but for storm-centric data rather than all-conditions data.

ACPD
13, 11971–11995, 2013

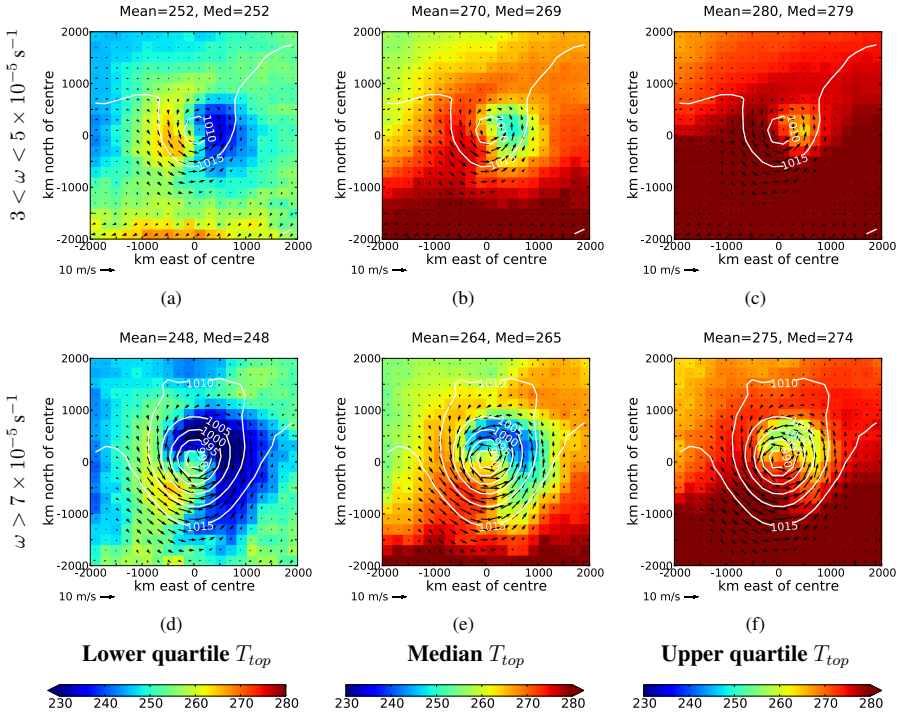

Fig. 4. Similar to Fig. 1, but for Aqua-MODIS cloud top temperature (T_{top}, K) over the North Atlantic ocean.

ACPD
13, 11971–11995, 2013

Contribution of cyclones to cloud–aerosol relationships

B. S. Grandey et al.

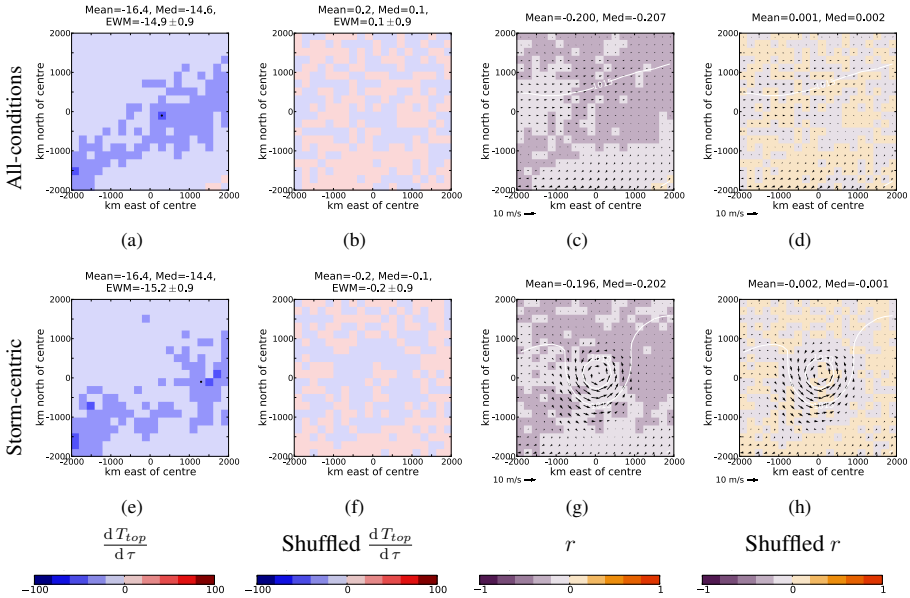

Fig. 5. Similar to Fig. 3, but for ordinary least squares regression fits of cloud top temperature (T_{top}, K) versus aerosol optical depth (τ) over the North Atlantic ocean.

ACPD
13, 11971–11995, 2013

Contribution of cyclones to cloud–aerosol relationships

B. S. Grandey et al.